

Performance assessment of wake mitigation strategies

M Coquelet^{1,2}, M Moens¹, L Bricteux², J-B Crismer¹, P Chatelain¹

¹ Institute of Mechanics, Materials and Civil Engineering, Université catholique de Louvain, 1348 Louvain-la-Neuve, Belgium.

² Fluids-Machines Department, Université de Mons, 7000 Mons, Belgium.

E-mail: marion.coquelet@uclouvain.be

Abstract. Many control strategies have emerged in the field of wind energy to address wake interaction effects and try to maximize wind farm power production. They rely either on wake redirection or on induction control. While wake redirection is easily performed by yawing the turbine, efficient and practically deployable induction control is not as straightforward. Recent studies paved the way with periodic dynamic induction control (PDIC), a strategy that generates pulsatile patterns in the wake and increases wake remixing. This study aims at further investigating the physics behind PDIC through large eddy simulations at high resolution. Results show the wake shear layer destabilization leading to the pulsatile wake. This paper also presents a comprehensive comparison between greedy control, PDIC and static yaw. It focuses both on power and loads at the scale of a pair of in-line turbines. It shows that PDIC significantly increases fatigue loads and leads to moderate power gains, while properly oriented yaw leads to fatigue load reduction on the upstream turbine and noticeable increase of the power production.

1. Introduction

As wind turbines generate a wake behind their rotor, clustering them into wind farms creates an important challenge in terms of wake interaction. Current control strategies still maximize power extraction at a single turbine level. Power losses up to 60% have been reported for waked turbines compared to their free-stream counterparts [2]. Many investigations have therefore emerged in the field of wind energy to mitigate wake interaction effects and seek to maximize wind farm power production. Wake mitigation control relies on two main strategies: wake redirection and induction control. Wake redirection, as the name suggests, tackles the wake interaction challenge by deviating the wake of an upstream turbine from a downstream one. It is easily performed by yawing the upstream turbine and has shown promising results both in simulations and in experiments [8, 19]. When it comes to induction control, first investigations proposed to statically derate first-row turbines to reduce the intensity of their wakes and increase the available power for downstream turbines. The axial induction of the upstream turbine was reduced either by offsetting the collective pitch angle from the optimum setting or by increasing the generator torque given a certain multiplicative constant. Research based on high-fidelity simulations and wind-tunnel experiments has unfortunately revealed that static induction control barely provides power gains [1]. More recently, dynamic induction control (DIC) has raised interest, its principle being to reduce the length of the wake recovery process. This latter process starts when the shear layer at the edge of the wake, resulting from the significant difference of streamwise velocity inside and outside the wake, becomes unstable. Eddies are then formed and bring momentum from the outer flow into the wake, thus re-energizing it [14]. In the first study by Goit and

Meyers [12], DIC is achieved by dynamically changing the thrust coefficient of each turbine over time. The optimal thrust coefficients are determined using a receding-horizon optimal control approach and large eddy simulations in which turbines are modelled by actuator disks. The studied 10x5-turbine wind farm yields energy extraction gains up to 16%. The work is extended to the study of finite wind farms in Goit et al. [13] and shows more moderate results, with power gains around 7%. Similar gains (8.21%) are also reported in Munters and Meyers [17], who applied the methodology presented in Goit and Meyers [12] to a 12x6-turbine wind farm. Also, simulation results showed that fast variations in turbine thrust coefficients are not a prerequisite for significant gains in energy extraction. Yilmaz and Meyers [21] built on previous work to bring a major novelty: the control variable is not the thrust coefficient any more, but the generator torque and blade pitch, making it closer to practical implementation. In the study, a simple uniform inflow case is first considered for which the optimal control leads to 25% gains. The optimal generator torque and blade pitch controls are further synthesized into a signal that can be periodically used as an open-loop controller and is tested in turbulent inflows. Results show that wake forcing is most successful in lower turbulent environments, where dynamic forcing can compensate for the lack of natural unsteadiness. For moderate turbulence intensities, power gains were observed to be between 2% and 7%. Another step towards practical implementation is taken in Munters and Meyers [18], as the authors aim to identify simplified control strategies that mimic the optimal control results. They show that optimal controls for first-row turbines increase wake mixing through the periodic shedding of vortex rings and that this behavior can be reproduced with a simple sinusoidal thrust control strategy. A grid search with different amplitudes and frequencies is performed to find the periodic signal that results in the maximum energy extraction. A similar grid search is carried through wind tunnel experiments in Frederik et al. [11], where the thrust coefficient variations are practically implemented through sinusoidal variations of the collective pitch angle. Similar power gains of a few percents are observed in the numerical results of Munters and Meyers [18] and the experimental ones of Frederik et al. [11] for these periodic induction control (PDIC) strategies. While power gain has long been the only variable of interest in DIC studies, recent work by Frederik and van Wingerden [10] has focused on the load impact of such strategies, which significantly increase the damage equivalent load on the blades and tower of the turbine.

The present study aims at further investigating PDIC, (1) in terms of wake dynamics and (2) in terms of power gains and extra-loads at the scale of a pair of turbines. A first analysis is held at the scale of a single turbine using high-fidelity large eddy simulations (LES), both in uniform and turbulent wind conditions, using discrete blade-type representation. Few simulations of this type have been proposed in the literature so far when it comes to (P)DIC. In order to enable a comparison with more common wake mitigation strategies, the LES of a single turbine in static yaw configurations is also performed in turbulent wind conditions. The second analysis of the paper is based on the pair of turbines and consists in a comparison between greedy control, PDIC and static yaw regarding both power and loads. Such a comprehensive approach, comparing different strategies in identical wind conditions, is necessary to better understand the implications of deploying one strategy or another in operating wind farms. It also allows to identify their shortcomings and therefore shed light on aspects that need to be improved in further investigations.

The paper is structured as follows: section 2 presents the methodology, section 3 describes the numerical set-ups, results of the first and second analyses are provided in section 4 and conclusions are drawn alongside perspectives in section 5.

2. Methodology

This section presents the in-house Large Eddy Simulation (LES) tool used for the numerical experiments as well as the implemented control schemes.

2.1. Numerical solver

Simulations are performed with a Vortex Particle-Mesh Method (VPM) [6] in which the Navier-Stokes equations are solved in their vorticity-velocity formulation. Blades are modelled by immersed lifting lines (ILL) [5] and the turbine dynamics are computed by the multi-body-system solver ROBOTRAN [7]. Turbulence is injected at the inflow using Mann boxes [16]. Atmospheric shear is modelled through an analytical exponential shear law reading $\frac{U(y)}{U_{ref}} = \left(\frac{y}{H_{hub}}\right)^\alpha$, where y is the vertical elevation from the ground, H_{hub} and U_{ref} are the hub height and velocity respectively and α is the shear coefficient.

2.2. Controllers

First of all, a standard Maximum Power Point Tracking (MPPT) controller [15] is used for all turbines, whatever their operating conditions. It relies on a generator-torque controller, maximizing the power capture below rated wind speeds, and a collective blade pitch controller, regulating the rotor speed above rated wind speeds to maintain nominal power production.

When periodic dynamic induction control (PDIC) is tested, it is implemented as a superimposition of low-frequency harmonic oscillations onto the collective pitch angle β_{MPPT} computed by the background MPPT controller. The optimal parameters of the harmonic oscillations are found in [9, 18]: $St = fD/U_{ref} = 0.25$ and $A = 2.5^\circ$ where St is the Strouhal number, D is the rotor diameter, U_{ref} is the mean wind speed and f and A are respectively the frequency and amplitude of the pitch oscillations. Eventually, the pitch angle evolution is dictated by

$$\beta_{CPC} = \beta_{MPPT} + A \sin\left(2\pi St \frac{U_{ref} t}{D}\right). \quad (1)$$

In some cases, an additional control loop targeting load alleviation is also added. More precisely, individual pitch control (IPC) in its mostly-used form [4] is implemented. The pitch angle of each blade b therefore becomes $\beta_b = \beta_{CPC} + \Delta\beta_{IPC,b}$, where $\Delta\beta_{IPC,b}$ is the pitch angle correction that insures the reduction of the once-per-revolution (1P) load oscillations. We highlight that PDIC and IPC pitch oscillations appear at distinct frequencies and can therefore be superimposed as mentioned here. Indeed, when operating at under-rated wind speeds (region 2), the MPPT controller insures a constant tip-speed ratio of 7.55 [15], thus leading to a Strouhal number of the IPC oscillations of 2.4, i.e. 10 times bigger than the PDIC ones.

3. Numerical setups

Simulations of the NREL 5MW [15] are performed at $U_{ref} = 9$ m/s, i.e. the turbine operates at under-rated wind speed and optimization related to wake interaction is much needed. Two sets of inflow conditions are used: (1) a uniform inflow case and (2) a case displaying a turbulence intensity $TI = 6\%$ with a shear coefficient $\alpha = 0.2$. The Mann box generated has a length of $32D$ and statistics are computed over that extent. The choice for moderate TI allows for wake mixing strategies to still offer a benefit [21]. We define x as the streamwise direction, y as the upward vertical direction and z as the transverse direction. The turbine rotates positively around the downstream-pointing x -direction (see Fig. 1(a)).

For the first analysis focusing on flow physics, we perform the high resolution LES of a single wind turbine operated using MPPT and PDIC. For each control case, both the uniform inflow and the turbulent and sheared inflow are simulated. In order to put forward the elements necessary for the performance analysis, we also perform the simulations of a single yawed turbine with yaw angles -20° and $+20^\circ$ in the turbulent case only. Note that the yaw angle γ is defined positively around the upward vertical direction y (see Fig. 1(b,c)). For all the single turbine cases, the numerical domain has dimensions of $12D \times 3D \times 4D$ with an homogeneous spatial resolution $h = D/64$, leading to about 38 million points. The boundary conditions are inflow-outflow

in the streamwise direction, slip wall in the vertical direction and periodic in the transverse direction. Although not presented in this paper, we verify that the spanwise periodicity is not problematic when relatively comparing quantities of interest such as power or fatigue loads. The simulations are run on massively parallel supercomputers using IvyBridge CPUs and the cost of each simulation is close to 3500 CPU×hours. The total computational cost of the 6 simulations therefore reaches 21000 CPU×hours.

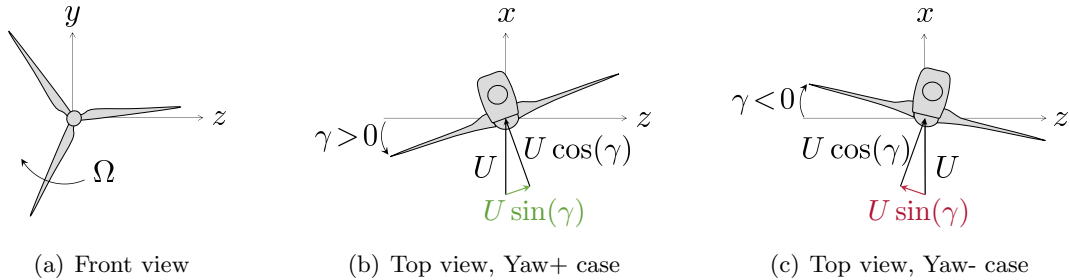


Figure 1. Numerical setup: reference frame, direction of rotation and yaw angle convention.

For the second analysis targeting performance assessment, we simulate a pair of in-line turbines in the turbulent and sheared inflow conditions. While the downstream turbine (WT2) is always operated at MPPT, 4 control cases are tested for the upstream one (WT1): MPPT (Ref), PDIC, positive yaw of $\gamma = 20^\circ$ (Yaw+) and negative yaw $\gamma = -20^\circ$ (Yaw-). For these 4 control cases, we envision 3 streamwise turbine spacings, namely $5D$, $6D$ and $7D$. Eventually, we envision the use of IPC for two additional cases that will be presented in the results section. This leads to a total of 14 simulations. In order to maintain affordable computational costs, we opt for a coarser spatial resolution with $h = D/32$. The latter, with a domain of dimension $14D \times 3D \times 4D$, leads to 5.5 million points. The cost of each simulation is lowered to 400 CPU×hours, therefore resulting in a total computational cost for this parametric study of 5600 CPU×hours. Though out-of-scope of this paper, we obtain conclusive results when verifying that the coarser resolution allows to capture the physics we are interested in.

4. Results

This section is organized as follows: we first define some quantities of interest that will be used for diagnostics, we then present the results of the single turbine simulations and we finally discuss the results of the pair of turbines.

4.1. Quantities of interest

First, we present the three following operators: for any quantity of interest ϕ , $\langle \phi \rangle$ stands for the spatially-averaged value, $\bar{\phi}$ is the temporal average and $\Delta_{rel}(\phi) = \frac{\phi - \phi_{ref}}{\phi_{ref}}$ is the relative increase of the quantity with respect to its value in the reference control case.

We then recall standard machine indicators, namely the thrust coefficient C_T , the power coefficient based on the aerodynamic power C_{P_a} and the power coefficient based on the electrical power C_{P_e} , respectively as

$$C_T = \frac{T}{\frac{1}{2}\rho U_{ref}^2 A}, \quad C_{P_a} = \frac{P_a}{\frac{1}{2}\rho U_{ref}^3 A}, \quad C_{P_e} = \frac{P_e}{\frac{1}{2}\rho U_{ref}^3 A}, \quad (2)$$

where ρ is the air density, U_{ref} is the mean infinite upstream velocity, $A = \pi D^2/4$ is the rotor swept area, T is the rotor thrust force, P_a is the aerodynamic power, P_e is the electrical power.

When it comes to loads, we use Damage Equivalent Loads (*DEL*) as defined in Hansen [14] to characterize the fatigue resulting from a varying moment $M(t)$.

Eventually, to quantify the wind power available in the wake of a turbine for a possible downstream turbine, we define $P_w = \frac{1}{2}\rho\langle u_x \rangle^3 A$, where $\langle u_x \rangle$ is the spatially-averaged value of the streamwise velocity field u_x within a disk of diameter D located at hub height.

4.2. Wind turbine and wake behavior under periodic dynamic induction control

This first analysis discusses the simulation of a single turbine. It focuses on the wake destabilization process using PDIC, the impact it has on the power available in the wake and the way the pulsatile behavior is generated at the rotor.

4.2.1. *Flow visualisation* Figure 2 shows the instantaneous streamwise velocity field at 5 instants over a pulsing period $T = \frac{D}{StU_{ref}}$, namely at $\frac{t}{T} = [0, \frac{1}{4}, \frac{1}{2}, \frac{3}{4}, 1]$. Results are presented for a theoretical case in uniform inflow to ease the discussion of the realistic case considering turbulence and shear.

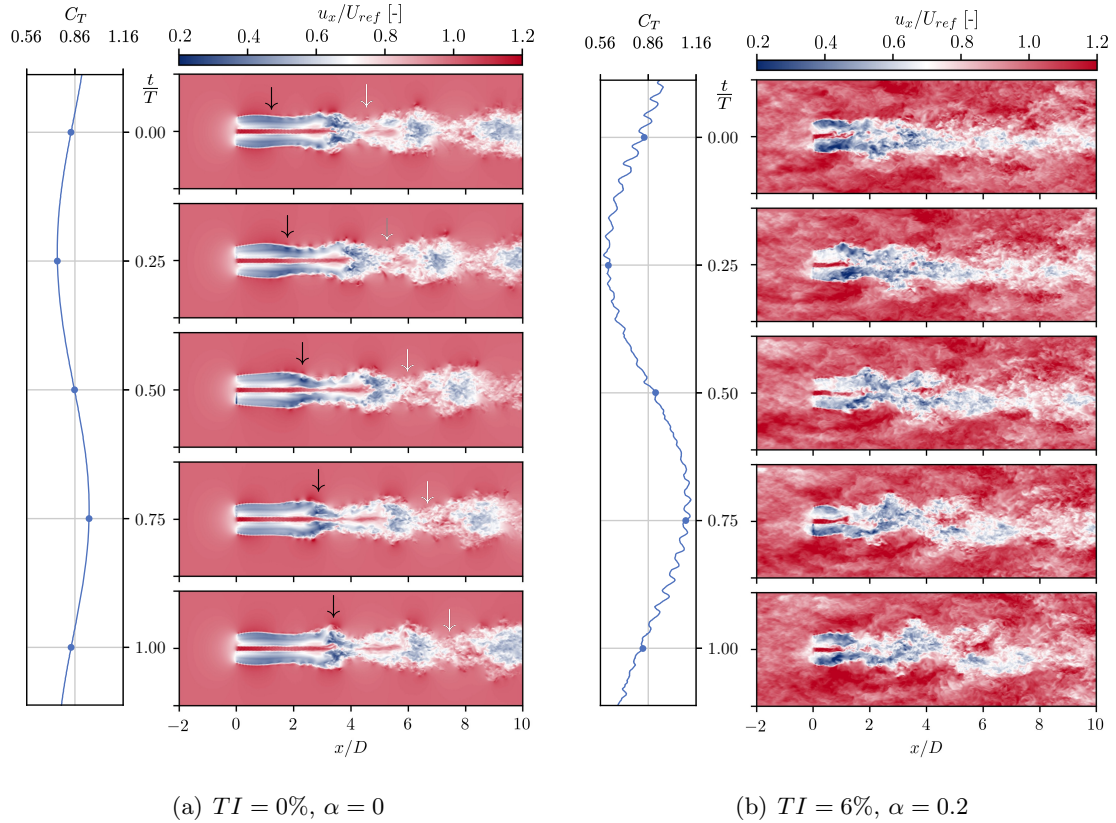


Figure 2. Top view of the instantaneous streamwise velocity field for a reference case without turbulence nor shear and a realistic case with turbulence and shear.

As mentioned before, wake recovery starts when the shear layer present at the edge of the wake becomes unstable. The intensity of that shear layer is a direct translation of the wake deficit and thus of the turbine induction. In the case of PDIC, the intensity of the shear layer periodically varies, which fastens its destabilization. In Fig. 2(a), one can observe the effects of the induction variations with alternating low- and high-velocity zones just behind the rotor ($[0, 2D]$). The shear layer destabilization (black arrows) produces an increased entrainment and re-energization of the

wake. Indeed, the velocities induced by the underlying vortical structures bring the outer flow velocities closer to the wake axis (x -axis) at the locations directly downstream of the structures shed by an increasing thrust (white arrows). The wake, which we will refer to as pulsatile wake, even breaks up into a sequence of distinct low-velocity pockets. With high-speed flow continuing to penetrate into the wake core, the detached zone (downstream of the break-up) is pushed faster downstream, while the advection of the attached zone (upstream of the break-up) is slower. As a result, the streamwise extent of the high velocity zone increases, leading to potential power gains for a downstream rotor.

As turbulence helps the wake recovery process, the phenomena described for the uniform case are not the sole source of instability any more in the turbulent case. Though some pulsatile patterns can still be observed (Fig. 2(b)), the wake is clearly not as markedly pulsatile as in the uniform case. This means that, in turbulent conditions, PDIC mainly helps destabilizing the wake. This is positive in a wind farm perspective, as the wake should not be more damaging for a second turbine than in usual operating conditions. That will be discussed in the second part of the results section.

4.2.2. Quantitative wake analysis The pulsatile behavior of the wake has been demonstrated. Figure 3 now shows the gains it can lead to in turbulent conditions. The mean velocity profiles in the wake show a slightly faster wake recovery when PDIC is used. As the gains in available power in the wake scale as the cube of the streamwise velocity, the little velocity gains translate into wake power gains close to 12.5% in the zone ranging from $5D$ to $7D$, where a second turbine is typically located in a wind farm configuration. In the second part of the results section dedicated to the 2-turbine wind farm analysis, we will quantify how much of this extra power is a second turbine capable of extracting and what is the resulting power production of the farm.

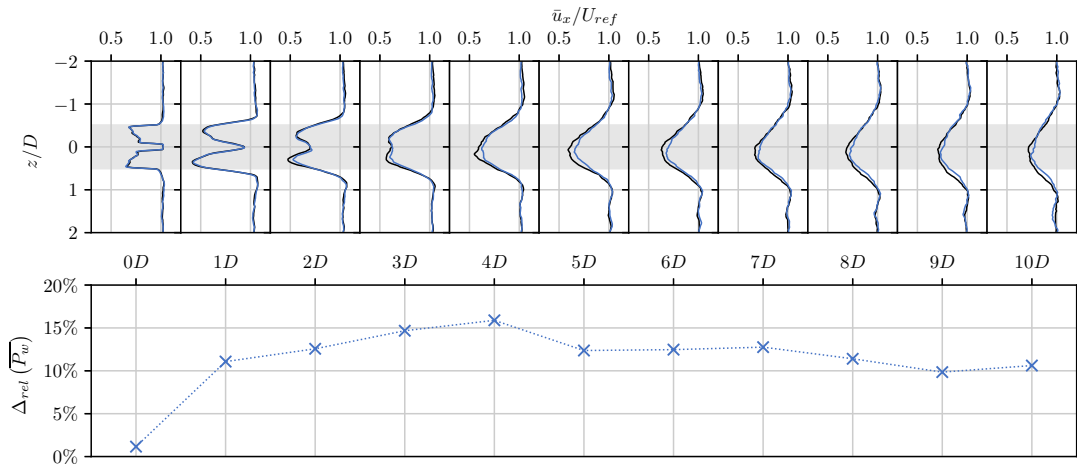


Figure 3. Quantitative wake analysis in turbulent and sheared wind conditions: (top) time-averaged velocity profile in a horizontal plane located at hub height for the reference case (black) and the PDIC case (blue), the shaded area represents the extent of a potential downstream rotor; (bottom) gain in the wind power available in the wake using PDIC.

4.2.3. Operating parameters This paragraph describes how the typical pulsatile behavior of the wake is generated at the rotor and how it compares with a rotor simply operating at MPPT. Only the realistic turbulent cases are presented. Fig. 4(a) shows the evolution of the pitch angle

β , which is invariably equal to zero for the reference case (black) but is purely sinusoidal in the PDIC case (blue). Fig. 4(b) displays the evolution of the rotation speed. In the reference case, it slightly evolves with the passage of gusts and lulls, which respectively allow to accelerate the rotor or force it to decelerate. Once PDIC is activated, oscillations clearly appear at the pulsing frequency. When the blades pitch in ($\beta \nearrow$), the wind load decreases and the turbine decelerates. On the contrary, when the blades pitch out ($\beta \searrow$), the rotor harvests more energy from the wind and can accelerate. The evolution of the thrust coefficient C_T , real marker of the induction, is presented in Fig. 4(c). Looking at the reference case, one can notice low-frequency and high-frequency oscillations. The low-frequency ones are due to the computation of C_T , which is based on the time-invariant reference velocity U_{ref} . If C_T were to be defined towards the velocity really imping the rotor at each instant, these low-frequency oscillations would vanish as the turbine operates in region 2 of control where C_T is constant [15]. The high-frequency oscillations can be attributed to the shear present in the simulation. Indeed, in such conditions, the forces acting on each blade are characterized by 1P oscillations. When the three forces normal to the rotor plane are summed, the resultant thrust force T displays 3P (three-times-per-revolution) oscillations. The evolution of C_T in the PDIC case shows an additional feature: it greatly oscillates at the pulsing frequency to generate the dynamic induction (this generates additional fatigue on the structural components and will be discussed later). One also notices that C_T responds almost immediately to the actuation of β , though the two are in opposition of phase as increasing the pitch reduces the thrust force. Fig. 4(d) finally presents the evolution of the power coefficients. While the remarks related to C_T hold for C_{P_a} (thin line), C_{P_e} (thick line) does not display high-frequency oscillations as it results from the generator torque, itself computed from the low-pass filtered rotation speed. It is interesting to note the time shift between the aerodynamic power and the electrical power, due to the rotor inertia. The shift increases for the PDIC case as the rotor accelerations are larger, leading to bigger inertial effects.

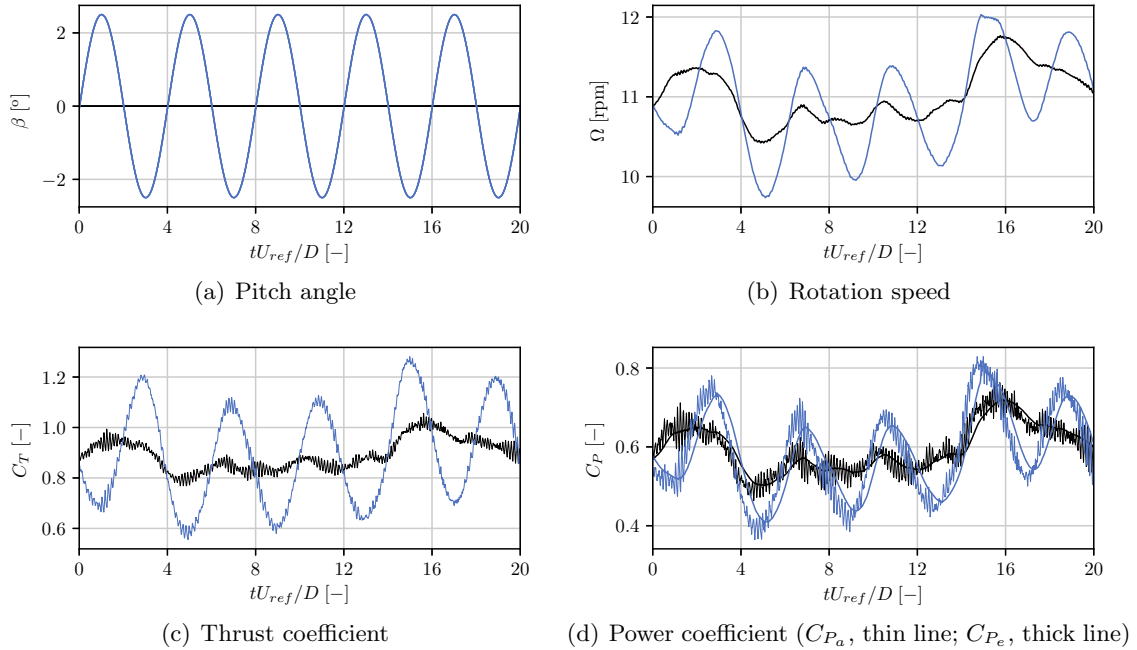


Figure 4. Temporal evolution of operating parameters for the reference control case (black) and the PDIC case (blue) over five pulsing period $T_{PDIC} = 4D/U_{ref}$ in turbulent flow conditions.

4.3. Wind turbine and wake behavior under static yaw control

While the previous section offers an insight into the physics of pulsatile wakes, this section recalls fundamental results regarding steered wakes [3] to ease the discussion of the performance assessment analysis. Attention is paid to the differences in wake behavior depending on the direction of the yaw angle under turbulent and sheared conditions.

4.3.1. Flow visualisation Figure 5 shows the time-averaged streamwise velocity field in vertical slices taken $6D$ downstream of the rotor of an aligned turbine (Ref), a positively yawed one (Yaw+) and a negatively yawed one (Yaw-). Given the yaw angle definition, the wake is displaced in the negative z direction for the Yaw- case and in the positive z direction for the Yaw+ case.

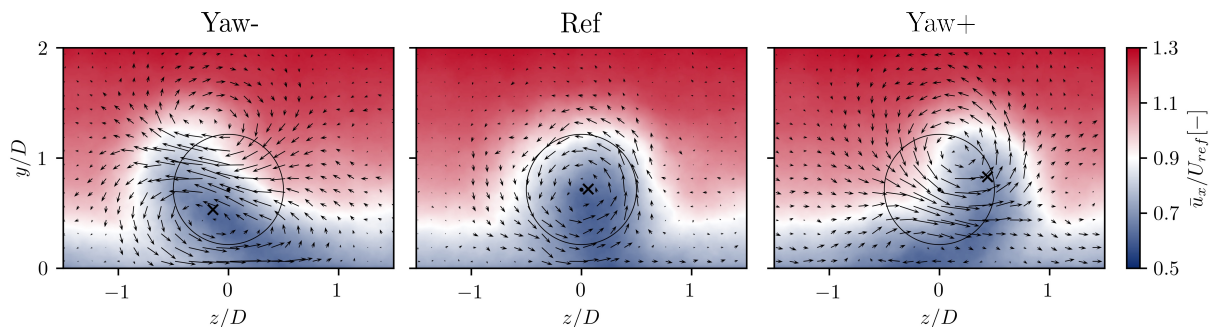


Figure 5. Front view of the temporally averaged streamwise velocity field in turbulent and sheared wind for $\gamma = -20^\circ$ (Yaw-), $\gamma = 0^\circ$ (Ref) and $\gamma = 20^\circ$ (Yaw+). The slice is taken $6D$ downstream of the turbine. Black circles indicate the frontal area of a possible downstream turbine whose center is the black dot. Arrows represent the projection of the velocity field onto the slice plane. Black crosses denote the wake center position.

While the wake deficit of the aligned turbine has a Gaussian-like shape, steered wakes exhibit what is known in the literature as the kidney shape [3]. This specific shape is attributed to the counter-rotating vortex pair (CVP) formed as the wake moves downstream. The formation of these CVP is detailed in [3] and their orientation depends on the yaw angle orientation. The CVP interacts with the vortex associated with the wake rotation (see Fig. 5 Ref), the latter rotates in the opposite direction of the turbine blades as it results from the reaction torque exerted by the blade onto the fluid. What explains the asymmetry between the Yaw+ and Yaw- cases is the interaction between the CVP and the wake rotation vortex. The resulting vortex system tends to displace the wake center not only laterally, but also vertically. As in [3], we show in Fig. 5 that the wake center is displaced downward and the Yaw- case, while it is displaced upward in the Yaw+ case. Also, the wake center displacement is slightly smaller in the negative yaw case than in the positive one. A final comment concerns what happens in the circular zone corresponding to a potential downstream rotor (black circle). The dominant vortical structure in that zone is the resulting downward vortex in the Yaw- case but the upward one in the Yaw+ case. This implies that momentum is mostly injected from lower areas of the boundary layer (low velocity) in the first case, but from higher areas (high velocity) is the second case. This suggests that the Yaw+ case might be more favourable for a downstream turbine.

4.3.2. Quantitative wake analysis Figure 6 shows a quantitative analysis stemmed from the previous observations. The horizontal velocity profiles (top) further stress that the wake is more deflected from the x -axis in the Yaw+ case. When it comes to the wind power available through a downstream disk located in-line with the turbine (bottom), the Yaw+ case leads to significantly higher wind power. Gains are around 45% in the $5D$ to $7D$ zone compared to around 32% in

the Yaw- case. This confirms the intuition presented before related to the vortex dynamics in the wake: the injection in the disk zone of high velocity flow in the Yaw+ case is favourable.

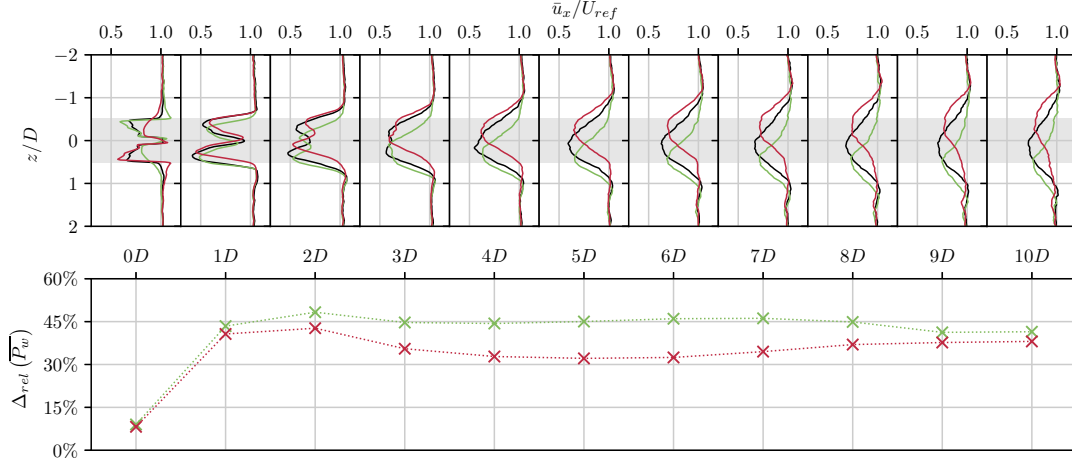


Figure 6. Quantitative wake analysis in turbulent and sheared wind conditions: (top) time-averaged velocity profile in a horizontal plane located at hub height for the reference case (black), the Yaw+ case (green) and the Yaw- case (red), the shaded area represents the extent of a potential downstream rotor; (bottom) gain in the wind power available behind the yawed rotor.

4.4. Performance assessment of wake mitigation strategies for a pair of in-line turbines

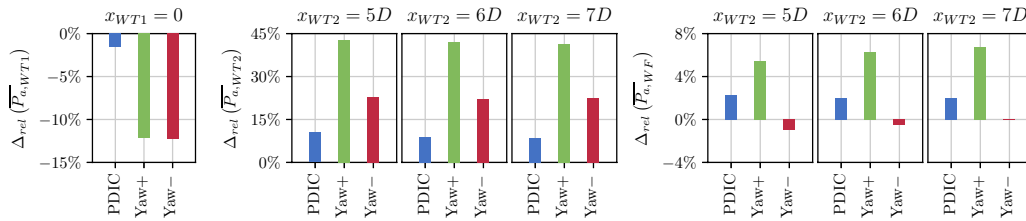
This part of the results section is organized as follows: we first present the impact of the multiple wake mitigation control strategies in terms of power and fatigue loads, we then discuss the most interesting cases and consider two additional configurations using IPC to alleviate fatigue loads.

4.4.1. Power production We first comment the results in terms of power production for each turbine individually (Fig. 7(a)). When PDIC is active on WT1, its mean power production is barely affected (-1%) and the pulsatile wake recovers faster, leading to a WT2 power increase going from 10% to 8% for the $5D$ to $7D$ spacings. This is relevant with the results of Fig. 3, which showed stable power gains close to 13% from $5D$ to $6D$ in the wake of a single turbine. The extra power in the wake is thus fairly well exploited by WT2. When WT1 is positively yawed, its power is reduced by 12% , but the wake deviation enables an extra 42% of power capture for WT2, whatever its spacing with WT1. This implies that WT2 exploits the extra power in the wake ($+45\%$ in Fig. 6) very well. When the yaw angle is negative, the power loss on WT1 is quite similar to that of the Yaw+ case, yet the power increase of WT2 plateaus around 22% . This limited gain partially finds an explanation in the fact that the wake deviation is not as efficient, as discussed before. Still, WT2 does not seem to totally exploit the 32% of extra power present in the negatively yawed wake shown in Fig. 6.

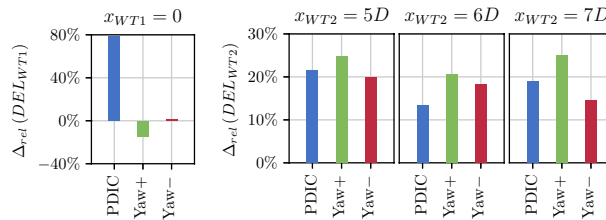
At the farm scale, the power gains are the following: for the PDIC case, the total power increases range from 2.3% to 1.9% ; for the positive yaw case, we observe power gains ranging from 5.4% to 6.7% ; for the negative yaw case, small power losses are observed, ranging from -1.0% to 0.0% . The global trend for yaw cases is that the bigger the spacing between WT1 and WT2, the more beneficial the wake redirection. That trend might be counter-intuitive as the power gains on WT2 are almost identical for the three downwind cases. Actually, the absolute production of WT2 increases between $5D$ and $7D$ as the wake is further dissipated. In the reference case,

the relative contribution of WT2 to the farm production is respectively 31%, 33% and 35% for the $5D$, $6D$ and $7D$ spacings. The impact of the relative power gains on the second turbine are thus intensified at the farm scale when WT2 is further away from WT1.

4.4.2. Fatigue loads This section is concerned with the load impacts, both on WT1 and WT2, of the wake mitigation strategies (Fig. 7(b)). Focusing on WT1 first, we recover recent results from Frederik et al. [10] showing a dramatic increase in flapwise fatigue for the PDIC case (+79%) due to the low-frequency oscillations of the thrust force. When it comes to yaw, similar results to those of Wang et al. [20] are recovered: positively yawing the turbine counterbalances the effects of shear, while negatively yawing it increases them. The peak-to-peak amplitude of the azimuthally-averaged flapwise loads, though not shown here, is reduced for Yaw+ and increased for Yaw-. Intuitively, this would suggest increased DELs for the Yaw+ case and decreased ones for the Yaw- case. However, as the fatigue analysis relies on counting cycles using the rainflow algorithm, the effects of turbulence, and not on shear only, are accounted for. In this case, the flapwise fatigue is reduced by 15% using Yaw+ but barely increased (+1%) with Yaw-. Now looking at the effects on WT2, loads are increased between 13% and 22% when PDIC is used. When WT1 is yawed, the wake in only partially deviated from WT2 and the partial wake impingement generates extra loads on WT2. One can note that, in the present case, the positively yawed wake seems more damaging than the negatively yawed one. These results should further be investigated but this is out of the scope of this analysis.



(a) Power production of each turbine (P_{WT1} , P_{WT2}) and cumulated (P_{WF} .)



(b) DEL associated to the flapwise bending moments for each turbine (DEL_{WT1} , DEL_{WT2}).

Figure 7. Relative impact of PDIC (blue), Yaw+ (green) and Yaw- (red) compared to Ref in terms of power and fatigue, for different spacings between the two turbines. For each spacing, the reference used for relative increase/decrease consists in the Ref case at that specific spacing.

4.4.3. Discussion and complementary cases Previous results have shown that the Yaw- case is not a good option, as it mostly leads to the power losses at the pair scale and increases loads on both turbines. It will therefore not be discussed anymore. The Yaw+ case is more promising: it generates significant power gains (even more significant when WT2 is further downstream) and reduces loads on WT1. Its only drawback is that it generates extra fatigue on the second turbine. The physics implied in the PDIC case makes it appealing in theory, but it generates a

significant increase in fatigue on the pulsing turbine and results in moderate power gains.

We investigate two additional cases that aim at limiting the negative side effects of PDIC and Yaw+. We opt for the 5D spacing as it is the one for which PDIC and Yaw+ compete in terms of wind farm power production. When WT2 is further downstream, Yaw+ results in significantly larger power gains than PDIC at the farm scale and should be preferred. The drastic increases in fatigue associated to PDIC on WT1 and to Yaw+ on WT2 open the discussion about whether or not IPC should be used, even though usually not active for under-rated wind speeds [20]. We therefore decide to activate IPC on WT1 in the PDIC case (we call that case PDIC*) and on WT2 for the Yaw+ case (we call that case Yaw+*). Results are presented in Tab. 1. In the PDIC* case, while IPC cuts about 30% of the extra fatigue loads on WT1, it also leads to further power losses on WT1 and reduced efficiency of the wake remixing process. Eventually, the global production is unchanged compared to the Ref case. The use of IPC is thus not relevant in this case. In the Yaw+* case, the activation of IPC on the second turbine is very beneficial in terms of loads, with DEL even lower than in the reference case. However, as for the previous case, activating IPC results in small power losses. The global power production of the Yaw+* is thus not as high as that of the Yaw+ one, yet it remains slightly higher than in the Ref case.

	P_{WT1} [MW]	P_{WT2} [MW]	P_{WF} [MW]	DEL_{WT1} [MNm]	DEL_{WT2} [MNm]
Ref	3.35 (ref)	1.58 (ref)	4.92 (ref)	1.71 (ref)	1.75 (ref)
PDIC	3.30 (-1.5%)	1.74 (+10.4%)	5.04 (+2.3%)	3.05 (+78.8%)	2.13 (+21.5%)
PDIC*	3.19 (-4.7%)	1.73 (+9.8%)	4.92 (-0.1%)	2.55 (+49.7%)	2.06 (+18.0%)
Yaw+	2.94 (-12.1%)	2.25 (+42.9%)	5.19 (+5.4%)	1.46 (-14.5%)	2.18 (+24.7%)
Yaw+*	2.94 (-12.1%)	2.08 (+31.8%)	5.02 (+2.0%)	1.46 (-14.5%)	1.62 (-7.4%)

Table 1. Focus on 5 control cases: Ref (both turbines operate at MPPT), PDIC (WT1: PDIC, WT2: MPPT), PDIC* (WT1: PDIC+IPC, WT2: MPPT), Yaw+ (WT1: Yaw+, WT2: MPPT), Yaw+* (WT1: Yaw+, WT2: MPPT+IPC).

5. Conclusions

In the first part of this study, we showed how PDIC fastens wake destabilization by periodically varying the intensity of the wake shear layer. We discussed the pulsatile pattern in uniform wind resulting from the wake break-up into low-velocity pockets. We highlighted that, in turbulent wind, the wake is not as markedly pulsatile and suggested that the shear layer destabilization is thus the main source of the power gains. We also recalled fundamental properties of steered wakes, like the interaction between the wake rotation and the CVP generated by yawed turbine, and highlighted the impact it has on wake redirection and on downstream power gains.

The second part of the study aimed at assessing and comparing the performances of these wake mitigation strategies in the case of a pair of in-line turbines. It showed that, both in terms of power production and fatigue loads, static yaw control, when wisely oriented, is a best candidate compared to PDIC as implemented so far. Indeed, wake steering does not have a detrimental effect on the loads of a turbine and valuably increases the power production of a downstream turbine. Its only drawback is the negative effect it has on the loads of the downstream machine due to the partial wake impingement. On the contrary, PDIC is impactful on the loads and leads to smaller power gains. IPC does not seem to be a good option to enhance PDIC performances as it does not counterbalance the low-frequency thrust oscillation impact on the loads and annihilates the small power gains. Further investigations on (P)DIC are thus necessary to make it competitive with wake steering. Properly phasing the pulsations with the incoming turbulent structures could be a first option.

Acknowledgments

This project has received funding from the European Research Council under the European Union's Horizon 2020 research and innovation program (grant agreement No. 725627) and from the Université de Mons under the 50/50 PhD funding program. This research benefited from computational resources made available on the Tier-1 supercomputer of the Fédération Wallonie-Bruxelles funded by the Walloon Region under the grant agreement No. 1117545 and on resources provided by the Consortium des Equipements de Calcul Intensif, funded by the Fonds de la Recherche Scientifique de Belgique under Grant No. 2.5020.11 and by the Walloon Region.

References

- [1] J. Annoni, P. Gebraad, A. Scholbrock, P. Fleming, and J.-W. van Wingerden. Analysis of axial-induction-based wind plant control using an engineering and a high-order wind plant model. *Wind Energy*, 2016.
- [2] R. Barthelmie, S.C. Pryor, S.T. Frandsen, K.S. Hansen, J.G. Schepers, K. Rados, W. Schlez, A. Neubert, L.E. Jensen, and S. Neckelmann. Quantifying the impact of wind turbine wakes on power output at offshore wind farms. *Journal of Atmospheric and Oceanic Technology*, 2010.
- [3] Majid Bastankhah and Fernando Porté-Agel. Experimental and theoretical study of wind turbine wakes in yawed conditions. *Journal of Fluid Mechanics*, 2016.
- [4] E. Bossanyi. Individual blade pitch control for load reduction. *Wind Energy: An International Journal for Progress and Applications in Wind Power Conversion Technology*, 2003.
- [5] D.-G. Caprace, P. Chatelain, and G. Winckelmans. Lifting line with various mollifications: theory and application to an elliptical wing. *AIAA Journal*, 2019.
- [6] P. Chatelain, M. Duponcheel, D.-G. Caprace, Y. Marichal, and G. Winckelmans. Vortex particle-mesh simulations of vertical axis wind turbine flows: from the airfoil performance to the very far wake. *Wind Energy Science*, 2017.
- [7] N. Docquier, A. Poncelet, and P. Fiset. Robotran: A powerful symbolic generator of multibody models. *Mechanical Sciences*, 2013.
- [8] P. Fleming, P. Gebraad, S. Lee, J.-W. van Wingerden, K. Johnson, M. Churchfield, J. Michalakes, P. Spalart, and P. Moriarty. Evaluating techniques for redirecting turbine wakes using sowfa. *Renewable Energy*, 2014.
- [9] J. Frederik, B. Doekemeijer, S. Mulders, and J.-W. van Wingerden. The helix approach: Using dynamic individual pitch control to enhance wake mixing in wind farms. *Wind Energy*, 2020.
- [10] J. Frederik and J.-W. van Wingerden. On the load impact of dynamic wind farm wake mixing strategies. *Available at SSRN 3910237*, 2021.
- [11] J. Frederik, R. Weber, S. Cacciola, F. Campagnolo, A. Croce, C. Bottasso, and J.-W. van Wingerden. Periodic dynamic induction control of wind farms: proving the potential in simulations and wind tunnel experiments. *Wind Energy Science*, 2020.
- [12] J. Goit and J. Meyers. Optimal control of energy extraction in wind-farm boundary layers. *Journal of Fluid Mechanics*, 2015.
- [13] J. Goit, W. Munters, and J. Meyers. Optimal coordinated control of power extraction in les of a wind farm with entrance effects. *Energies*, 2016.
- [14] M. Hansen. *Aerodynamics of wind turbines*. Routledge, 2015.
- [15] J. Jonkman, S. Butterfield, W. Musial, and G. Scott. Definition of a 5-mw reference wind turbine for offshore system development. Technical report, National Renewable Energy Lab.(NREL), 2009.
- [16] J. Mann. Wind field simulation. *Probabilistic engineering mechanics*, 1998.
- [17] W. Munters and J. Meyers. An optimal control framework for dynamic induction control of wind farms and their interaction with the atmospheric boundary layer. *Philosophical Transactions of the Royal Society A: Mathematical, Physical and Engineering Sciences*, 2017.
- [18] W. Munters and J. Meyers. Towards practical dynamic induction control of wind farms: analysis of optimally controlled wind-farm boundary layers and sinusoidal induction control of first-row turbines. *Wind Energy Science*, 2018.
- [19] J. Wagenaar, L. Machielse, and J. Schepers. Controlling wind in ecn's scaled wind farm. *Proc. Europe Premier Wind Energy Event*, 2012.
- [20] C. Wang, F. Campagnolo, and C. Bottasso. Does the use of load-reducing ipc on a wake-steering turbine affect wake behavior? *Journal of Physics: Conference Series*, 2020.
- [21] A. Yilmaz and J. Meyers. Optimal dynamic induction control of a pair of inline wind turbines. *Physics of Fluids*, 2018.